Enforcing causality in nonrelativistic equations of state at finite temperature

Constantinos Constantinou[1,*] and Madappa Prakash[2,†]

[1]*Institute for Advanced Simulation, Institut für Kernphysik, and Jülich Center for Hadron Physics, Forschungszentrum Jülich, D-52425 Jülich, Germany*

[2]*Department of Physics and Astronomy, Ohio University, Athens, Ohio 45701, USA*

(Received 22 February 2017; published 8 May 2017)

We present a thermodynamically consistent method by which equations of state based on nonrelativistic potential models can be modified so that they respect causality at high densities, both at zero and finite temperature (entropy). We illustrate the application of the method by using the high-density phase parametrization of the well-known Akmal–Pandharipande–Ravenhall model in its pure neutron matter configuration as an example. We also show that, for models with only contact interactions, the adiabatic speed of sound is independent of the temperature in the limit of very large temperature. This feature is approximately valid for models with finite-range interactions as well, insofar as the temperature dependence they introduce to the Landau effective mass is weak. In addition, our study reveals that in first-principle nonrelativistic models of hot and dense matter, contributions from higher-than-two-body interactions must be screened at high density to preserve causality.

DOI: 10.1103/PhysRevC.95.055802

I. INTRODUCTION

The precise determination of neutron star masses close to $2M_\odot$ [1,2], prospects of observing gravitational waves (GWs) from mergers involving binary neutron stars as in the recent detection of GWs from mergers of binary black holes [3,4], and the hope of observing a nearby core-collapse supernova (SN) with the several neutrino observatories currently in place have greatly strengthened the study of dense matter physics. Central to this study is the equation of state (EOS) of dense matter at both zero and finite temperature. Depending on the values of the baryon densities n and temperatures T reached in core-collapse supernovae, neutron stars from their birth to old age, and mergers of compact binary stars, several phases of matter may be encountered. At high densities and/or temperatures, these phases may consist of strangeness-bearing hadrons and/or quark matter [5].

Large-scale computer simulations [6–17] of the astrophysical phenomena mentioned above employing the microscopic physics input of model EOSs from both nonrelativistic and relativistic approaches have indicated the ranges of n/n_s, where $n_s \simeq 0.16$ fm^{-3} is the nuclear saturation density, T, and the net electron fraction $Y_e = n_e/n$ encountered. To enable simulations, EOSs that range over n/n_s up to 10, T up to 200 MeV, and Y_e up to 0.6 are required. These conditions imply an entropy per baryon S (in units of Boltzmann's constant k_B) of up to 200. In varying amounts the entropy is shared between the hadrons, leptons, and photons. For EOSs with only nucleonic components, $S_{\rm nuc}$ of up to 4–5 is not uncommon. In the homogeneous phase ($n \geqslant 0.1$ fm^{-3}) and using the EOS of Akmal–Pandharipande–Ravenhall (APR) [18], $S \leqslant 30$ with nucleons contributing about 5, leptons 15, and photons 10. The highest density at which $S \sim 200$ is about 0.01 fm^{-3} (at $T = 200$ MeV) with 95% of the contributions coming from leptons and photons. The dependence of these numbers on the electron fraction is, generally, very weak.

The focus of this paper is on the adiabatic speed of sound c_s in matter at high density and temperature. In hydrodynamical simulations, c_s represents a physical scale which controls the macroscopic evolution of matter. Thus, a quantitative knowledge of how c_s varies with n and T (or S) in models of hot, dense matter can shed light on the time development of involved hydrodynamical simulations. In physical systems, c_s cannot exceed the speed of light c. Nevertheless, many of the EOSs used to describe nucleonic matter have nonrelativistic underpinnings and therefore are inherently incapable of conforming to the requirement of causality owing to the lack of Lorentz invariance. (Relativistic field-theoretical approaches to dense matter automatically respect causality, and will not be addressed further in this work.) For some nonrelativistic EOSs, typically the softer ones, which struggle to support neutron star (NS) masses $\sim 2M_\odot$, the central densities of maximum-mass stars occur at $n_c > (8\text{–}10)n_s$ (see, e.g., Ref. [19]). Consequently, the causality requirement is only violated for densities beyond the validity of a nonrelativistic treatment which must be eschewed. The stiffer EOSs however, can lead to acausal behavior at densities and temperatures for which hadronic matter is expected to persist within a star. In some fortuitous cases, the matter may not become superluminal prior to n_c. However, a large and steady rise in the adiabatic speed of sound should suffice to cast doubt on a nonrelativistic treatment as finite-temperature effects may lead to acausality, as will be shown later in the paper.

Repulsive contributions to the energy per particle $E(u = n/n_s)$ that vary faster than linear in u give rise to acausal behavior at high densities. Thus, higher-than-two-body forces found necessary to achieve saturation at the empirical n_s with the empirical binding energy of symmetric nuclear matter (SNM) must screen themselves with progressively increasing density to ensure causal behavior. Following the suggestion in Ref. [20], causality was maintained through the use of $Bu^\sigma/(1 + B'u^{\sigma-1})$, where $\sigma > 1$, B is a constant of dimension

*c.constantinou@fz-juelich.de
†prakash@ohio.edu

energy, and B' is a dimensionless constant appropriately chosen to have c_s approach c from below, in the explorative study of Ref. [19]. This implied that self-screening of repulsive interactions at high density, while desirable, is not always guaranteed in nonrelativistic potential model calculations. The simple approach adopted in the above works to maintain causality also highlights the need to identify the origin of the needed self-screening mechanism in dense matter.

At the two-body level in the mean-field approximation, contributions to $E(u)$ arising from exchange interactions in dense matter can either be positive or negative depending on the nature of the exchanged meson [21]. For interactions between nucleons mediated by pseudoscalar π and scalar σ mesons, the exchange (Fock) terms provide positive contributions to the energy, whereas the corresponding direct (Hartree) terms are negative. Vector meson (ω and ρ) exchanges lead to negative contributions from the Fock terms (except in relativistic treatments at high densities for which positive contributions ensue owing to relativistic effects). In all cases, however, the Fock contributions are subdominant to the Hartree terms. In addition, the asymptotic high-density behavior of the energy per particle from the Fock terms is $u^{1/3}$ much weaker than u of the Hartree terms. For a comparison of the individual contributions to the total exchange energy in relativistic and nonrelativistic treatments, see, for example, Ref. [22]. In models with contact interactions which subsume the exchange interaction in a density-dependent effective mass, the kinetic energy per particle varies as $u^{5/3}$, which invariably leads to acausality at some high density.

Beyond the mean-field approximation (as for example in Brueckner–Hartree–Fock (BHF) treatments [23–27]), even two-body forces can give rise to contributions that grow with powers of u larger than 1 owing to the class of diagrams summed, and short-range (Jastrow) correlations in the wave functions. Higher-power attractive terms may result in such calculations that can help to delay the onset of acausality to densities larger than those found in the cores of neutron stars, but at the expense of making the EOS too soft to support a $2M_\odot$ star. In the case of higher-power repulsive terms, causality will be at stake likely at a density within the star. A detailed analysis of causality in such treatments with and without three-body forces, including that at finite temperature, is warranted but outside the scope of this work.

The issue of self-screening is particularly relevant to modern microscopic calculations of the EOS of SNM and pure neutron matter (PNM), such as the quantum Monte Carlo [28–30] and chiral effective field theory approaches [31–38] in which the role of three-body forces at $T = 0$ have been examined. Owing to inherent technical difficulties, calculations have been limited up to about $2n_s$ in both of these approaches. To calculate the structural properties of NSs, the EOSs have been extrapolated beyond $\sim 2n_s$ through the use of piecewise polytropes that respect causality (thus screening the influence of three-body forces present at $n < 2n_s$, possibly prematurely for higher densities) [39]. This polytropic extrapolation, while satisfactory at $T = 0$ on a practical level, cannot however be extended to finite temperature unless the effects of temperature on the EOS are known *a priori*. Examples of EOSs in which the role of three-body interactions at finite temperature have been investigated can be found in Refs. [40–42]. To our knowledge, tests of the causal behavior of these EOSs at high density and finite temperature have not been performed to date.

Here, we present a thermodynamically consistent method to maintain causality for EOSs that become acausal at both zero and finite temperature. While such a method is available in the literature for zero temperature [18,43,44], a method to encompass the influence of temperature on c_s has not received much attention (the method presented in Appendix E of our earlier work in Ref. [18] contained an inadvertent error, which is corrected in this work). We illustrate the application of the method by using a few chosen models [45–47] that become acausal at high density and temperature. These models have distinctly different behavior in their nucleon effective masses as functions of density. For simplicity, results for PNM are shown in all cases with the generalization to a multicomponent system indicated in the text. We stress, however, that the applicability of the method proposed is not limited to the class of models chosen for illustration. As long as the relevant thermodynamic variables such as the energy, pressure, and chemical potential for any model are available for all densities and temperatures of interest, the method can be used to render the EOS causal and to satisfy the thermodynamic identity.

The paper is organized as follows: In Sec. II, the adiabatic speed of sound c_s is defined in terms of thermodynamic quantities characteristic of an EOS at both zero and finite temperature. This section also contains a discussion of the behavior of c_s in the limiting cases of degenerate and nondegenerate bulk matter. The method devised to implement causality for EOSs that become acausal at high densities and temperatures is described in Sec. III. In Sec. IV, the numerical procedure to enforce causality for models with contact interactions is detailed. Results in the case of PNM for these models are presented in Sec. V both at zero and finite temperature. Additionally, results for a model in which contributions from higher than two-body interactions are screened to prevent an acausal behavior are presented. Section VI presents a summary and conclusions.

II. GENERAL CONSIDERATIONS

For small-amplitude perturbations, the velocity v of fluid particles obeys the wave equation [48]

$$\frac{\partial^2 v}{\partial t^2} - c_s^2 \frac{\partial^2 v}{\partial x^2} = 0, \tag{1}$$

whose solution $f(x - c_s t)$ represents longitudinal sound wave propagation with speed c_s under the condition of adiabatic motion for which $\partial S/\partial t = 0$, where S is the entropy. Thus, small density fluctuations in a compressible fluid propagate at the speed of sound given by [49–51]

$$\left(\frac{c_s}{c}\right)^2 = \left.\frac{\partial P}{\partial \epsilon}\right|_S = \frac{\partial P/\partial n|_S}{\partial \epsilon/\partial n|_S} \tag{2}$$

$$= \frac{1}{TS + \mu + m} \left.\frac{\partial P}{\partial n}\right|_S = \frac{K_s}{9(TS + \mu + m)} = \frac{\Gamma_S P}{h + mn}, \tag{3}$$

where P is the pressure, ϵ is the energy density, n is the number density, $h = nE + P$ is the enthalpy density, μ is the chemical potential, $K_S = 9\partial P/\partial n|_S$ is the adiabatic incompressibility, and $\Gamma_S = \partial \ln P/\partial \ln n|_S$ is the adiabatic index. In the variables (n,T), we can also express c_s as [50,52]

$$\left(\frac{c_s}{c}\right)^2 = \frac{C_P}{C_V}\frac{n}{h+mn}\left.\frac{\partial P}{\partial n}\right|_T, \tag{4}$$

where C_P and C_V are the specific heats at constant pressure and volume, respectively.

We will begin our analysis with nonrelativistic models that are described by the generic Hamiltonian density

$$\mathcal{H} = \frac{\hbar^2}{2}\frac{\tau(n,S)}{m^*(n)} + V(n), \tag{5}$$

where the first term is the kinetic-energy density and the second is the potential-energy density. The quantity m^* is the Landau effective mass defined at the Fermi surface by $m^*(n) = p_F/(\partial\epsilon_p/\partial p)|_{p_F}$, where ϵ_p is the single-particle spectrum and p_F is the Fermi momentum. Models that employ contact interactions such as Skyrme models, the APR model, and other microscopic models that employ the effective mass approximation as indicated above are examples of the representation in Eq. (5). As our discussion proceeds, we will consider other cases, e.g., models in which finite-range interactions at various levels of sophistication are considered and in which additional complications are encountered. Some physical insight is gained by examining the behavior of c_s in the limiting situations of degenerate and nondegenerate bulk matter to which we turn below.

A. Degenerate case

For conditions such that $T/T_F \ll 1$ (or, equivalently $S \leqslant 1$), where $T_F = p_F^2/(2m^*)$ is the Fermi temperature in nonrelativistic models, degenerate conditions prevail. In this case, the leading-order Fermi-liquid theory (FLT) expressions for the thermal components of the pressure and energy density are given by [53,54]

$$P_{th}(n,T) = \tfrac{2}{3}naT^2Q \text{ and } \epsilon_{th}(n,T) = naT^2, \tag{6}$$

$$\text{with } Q = 1 - \frac{3}{2}\frac{n}{m^*}\frac{dm^*}{dn}, \tag{7}$$

where $a = \pi^2/(4T_F)$ is the level density parameter. Utilizing the leading-order FLT result $S = 2aT$, we get

$$P_{th}(n,S) = \frac{S^2}{6}\frac{nQ}{a} = \frac{2S^2}{3\pi^2}nT_FQ, \tag{8}$$

$$\epsilon_{th}(n,S) = \frac{S^2}{4}\frac{n}{a} = \frac{S^2}{\pi^2}nT_F, \tag{9}$$

from which the density derivatives at constant S,

$$\left.\frac{dP_{th}}{dn}\right|_S = \frac{P_{th}}{n}\left(1 + \frac{2}{3}Q + \frac{n}{Q}\frac{dQ}{dn}\right),$$

$$\left.\frac{d\epsilon_{th}}{dn}\right|_S = \frac{\epsilon_{th}}{n}\left(1 + \frac{2}{3}Q\right),$$

$$\left.\frac{dT}{dn}\right|_S = \frac{2}{3}\frac{TQ}{n}, \tag{10}$$

are easily obtained. Putting together the other components in the total P and ϵ, we arrive at

$$\left.\frac{dP}{dn}\right|_S = \frac{2}{5}T_F\left(1 + \frac{2}{3}Q\right) + n\frac{d^2V}{dn^2} + \left.\frac{dP_{th}}{dn}\right|_S,$$

$$\left.\frac{d\epsilon}{dn}\right|_S = m + \frac{3}{5}T_F\left(1 + \frac{2}{3}Q\right) + \frac{dV}{dn} + \left.\frac{d\epsilon_{th}}{dn}\right|_S, \tag{11}$$

where the first term in the first equation above and the second term in the second represent the $T = 0$ results of the kinetic parts. These results allow us to appreciate how c_s^2 is governed by physical quantities in special circumstances.

(i) The case when $V = 0$: When the thermal contributions can be regarded as small ($S \leqslant 1$) compared to their zero-temperature counterparts,

$$c_s^2 \simeq \frac{2}{5}\frac{T_F}{m}\left(1 + \frac{2}{3}Q\right) \tag{12}$$

$$= \frac{1}{5}\left(\frac{p_F}{m^*}\right)^2\frac{m^*}{m}\left(1 + \frac{2}{3}Q\right). \tag{13}$$

The physical scale of c_s here is the velocity at the Fermi surface $v_F = p_F/m^*$ modified by m^*/m and its logarithmic derivative with respect to density contained in Q. For $m^*(n) = m$, the ideal-gas value of $c_s^2 = (1/3)(p_F/m)^2$ is recovered from Eq. (13).

(ii) Density-dependent $V(n)$: To achieve equilibrium at the empirical nuclear density $n_0 \simeq 0.16$ fm^{-3} with the empirical energy per particle of $\simeq -16$ MeV, and to support the precisely determined neutron star masses of $2M_\odot$, models of dense nuclear matter have employed contributions from beyond-two-body forces in $V(n)$ that vary as $n^{2+\epsilon}$. If these contributions persist at densities $n \gg n_0$ and dominate over the other contributions including the thermal parts ($S \leqslant 1$), causality is bound to be violated. Consider, for example, $V(n) \propto n^\sigma$ for which

$$\left(\frac{c_s}{c}\right)^2 \simeq \frac{nd^2V/dn^2}{dV/dn} = \sigma - 1, \tag{14}$$

which for $\sigma \geqslant 2$ renders $(c_s/c)^2 \geqslant 1$. Notice that the sign of $V(n)$, i.e., attractive or repulsive, drops out in this result. A combination of attractive and repulsive terms with different magnitudes and power-law behavior in n serves only to delay the onset of superluminal behavior.

(iii) Additional contributions to the density-dependent $V(n)$: As apparent from Eq. (11), both the $S = 0$ and $S \neq 0$ terms contribute in determining the magnitude of $(c_s/c)^2$. The interplay between these terms is also determined by $m^*(n)$ and its density derivatives as well as by $Q(n)$ and its derivatives. In Skyrme-like models in which $m^*/m = (1+\beta n)^{-1}$ with β a constant, the kinetic-energy density $\varepsilon_{kin} \propto n^{5/3}(1+\beta n)$, so that at some high n the $n^{8/3}$ term dominates causing the EOS to become acausal. In some cases, acausality can set in at lower densities for $S \neq 0$ than for $S = 0$. A quantitative discussion of results from

models with different behavior of m^*/m vs n will be deferred to Sec. V.

B. Nondegenerate case

At zero temperature (entropy), c_s is a function of just the density n. As we show below, the same is true for nonrelativistic models with only contact interactions in the limit of either very large entropy or temperature, i.e., the extreme nondegenerate limit. Here, the entropy is given by the Sackur–Tetrode relation

$$S = \frac{5}{2} - \ln\left[\left(\frac{2\pi\hbar^2}{m^*T}\right)^{3/2}\frac{n}{2}\right], \tag{15}$$

where m^* is the density-dependent Landau effective mass. Solving Eq. (15) for the temperature, we get

$$T = \frac{2\pi\hbar^2}{m^*}\left(\frac{n}{2}\right)^{2/3}\exp\left(\frac{2}{3}S - \frac{5}{3}\right), \quad \left.\frac{\partial T}{\partial n}\right|_S = \frac{2}{3}\frac{TQ}{n}, \tag{16}$$

with Q given by Eq. (7). In this case, thermal effects dominate over cold matter contributions (exclusive of rest mass) to thermodynamic properties. Consequently,

$$\left(\frac{c_s}{c}\right)^2 \overset{S\gg1}{\longrightarrow} \frac{\partial P_{th}/\partial n|_S}{m + \partial\varepsilon_{th}/\partial n|_S}. \tag{17}$$

For nonrelativistic contact-interaction models in the nondegenerate limit,

$$P_{th} = nTQ, \quad \left.\frac{\partial P_{th}}{dn}\right|_S = TQ\left(1 + \frac{2}{3}Q + \frac{n}{Q}\frac{dQ}{dn}\right), \tag{18}$$

$$\varepsilon_{th} = \frac{3}{2}nT, \quad \left.\frac{\partial\varepsilon_{th}}{dn}\right|_S = \frac{3}{2}T\left(1 + \frac{2}{3}Q\right). \tag{19}$$

When the mass term dominates over the thermal part in the denominator of Eq. (17), and $Q \simeq 1$ as is the case when the effects of interactions are small,

$$\left(\frac{c_s}{c}\right)^2 \overset{S\gg1}{\longrightarrow} \frac{5}{3}\frac{T}{m}, \tag{20}$$

which is the result for one-component classical gases. The physical scale of c_s here is the thermal velocity of particles. In the case that the thermal component of the denominator in Eq. (17) dominates over the mass,

$$\left(\frac{c_s}{c}\right)^2 \overset{S\gg1}{\longrightarrow} \frac{2}{3}\frac{Q\left(1 + \frac{2}{3}Q + \frac{n}{Q}\frac{dQ}{dn}\right)}{1 + \frac{2}{3}Q}, \tag{21}$$

that is, the temperature or entropy dependence drops out with the result $(c_s/c)^2 \simeq 2/3$ for $Q \simeq 1$. It must be emphasized that this result is obtained only at very high temperatures for which the use of nonrelativistic considerations becomes questionable.

C. Models with finite-range forces

Finite-range forces introduce momentum dependencies (other than p^2) to the single-particle potential which in turn cause it to acquire a temperature dependence [52]. The effects of these interactions can still be collected in a density- and temperature-dependent function $m^*(n,T)$ which, however, can no longer be identified with the Landau effective mass. Nevertheless, if this T dependence is weak, then

$$m^*(n,T) \simeq m^*(n,0) + T\left.\frac{\partial m^*(n,T)}{\partial T}\right|_{T=0} + \cdots \tag{22}$$

$$\equiv m^*(1 + bT), \tag{23}$$

where $m^* = m^*(n,0)$ is the Landau mass and $b(n) \equiv (1/m^*)\partial m^*(n,T)/\partial T|_{T=0}$ such that $bT \ll 1$. Combining Eq. (15) with $m^* \to m^*(n,T)$ and Eq. (23), and expanding in a Taylor series for $bT \ll 1$, we find

$$S \simeq \frac{5}{2} - \ln\left[\left(\frac{2\pi\hbar^2}{m^*T}\right)^{3/2}\frac{n}{2}\right] + \frac{3bT}{2}. \tag{24}$$

Perturbative inversion of Eq. (24) yields, in the second recursion,

$$T \simeq \frac{2\pi\hbar^2}{m^*}\left(\frac{n}{2}\right)^{2/3}\exp\left[\frac{2}{3}S - \frac{5}{3} - \frac{2\pi\hbar^2}{m^*}b\left(\frac{n}{2}\right)^{2/3}\exp\left(\frac{2}{3}S - \frac{5}{3}\right)\right]. \tag{25}$$

We now substitute $2\pi\hbar^2(n/2)^{2/3}\exp(2S/3-5/3)$ by $m^*(n,T)$, then replace $m^*(n,T)$ by $m^*(1+bT)$ to get

$$T \simeq \frac{2\pi\hbar^2}{m^*}\left(\frac{n}{2}\right)^{2/3}\exp\left[\frac{2}{3}S - \frac{5}{3} - \frac{bTm^*(n,T)}{m^*}\right] \simeq \frac{2\pi\hbar^2}{m^*}\left(\frac{n}{2}\right)^{2/3}\exp\left[\frac{2}{3}S - \frac{5}{3} - bT(1+bT)\right]. \tag{26}$$

Now dropping b^2T^2 and expanding the exponential for small bT,

$$T \overset{\substack{bT\ll1\\ S\gg1}}{\longrightarrow} \frac{2\pi\hbar^2}{m^*}\left(\frac{n}{2}\right)^{2/3}\exp\left(\frac{2}{3}S - \frac{5}{3}\right). \tag{27}$$

This result shows that, in the extreme nondegenerate limit, finite-range force models with weak T dependence in their m^* will behave similarly to zero-range models and thus they will also obey Eq. (21).

III. IMPLEMENTATION OF CAUSALITY

The general approach described below is more conveniently applied in the variables (n,S) that are natural to the speed of sound as opposed to (n,T) commonly used in tabulations of EOS properties. Working with the former set allows us to carry out all calculations analytically circumventing the need for numerical integration.

Causality is preserved as long as the speed of sound c_s is less than or equal to the speed of light c:

$$\left(\frac{c_s}{c}\right)^2 \equiv \beta = \left.\frac{\partial P}{\partial\epsilon}\right|_S = \left.\frac{\partial P}{\partial n}\right|_S\left(\left.\frac{\partial\epsilon}{\partial n}\right|_S\right)^{-1} \leqslant 1. \tag{28}$$

Here the total energy density ϵ is inclusive of the internal energy density ε and the rest-mass energy density mn:

$$\epsilon = \varepsilon + mn. \tag{29}$$

By making use of

$$P = n^2 \left.\frac{\partial(\epsilon/n)}{\partial n}\right|_{S,N} = n \left.\frac{\partial \varepsilon}{\partial n}\right|_{S,N} - \varepsilon \tag{30}$$

and

$$\left.\frac{\partial P}{\partial n}\right|_{S,N} = n \left.\frac{\partial^2 \varepsilon}{\partial n^2}\right|_{S,N}, \tag{31}$$

where N is the number of nucleons in the system, we write Eq. (28) as a second-order differential equation (DE):

$$\left.\frac{\partial^2 \varepsilon}{\partial n^2}\right|_{S,N} - \frac{\beta}{n}\left.\frac{\partial \varepsilon}{\partial n}\right|_{S,N} = \frac{\beta m}{n}. \tag{32}$$

Thus, in addition to entropy conservation, in our approach we must impose the condition of baryon number conservation and, in the case of multicomponent systems, fixed composition. Equation (32) can be reduced to a first-order DE

$$\left.\frac{\partial \xi}{\partial n}\right|_{S,N} - \frac{\beta}{n}\xi = \frac{\beta m}{n} \tag{33}$$

by setting

$$\xi = \left.\frac{\partial \varepsilon}{\partial n}\right|_{S,N} = \mu + TS. \tag{34}$$

Note that the combination of Eqs. (30) and (34) yields the thermodynamic identity $\varepsilon + P = n\mu + Ts$. The solution of Eq. (33) requires that β is mapped to some function $\beta_f(n,S) \leqslant 1\ \forall\ (n,S)$. This implies that the causality-fixing density n_f obtained from

$$\beta(n,S) - \beta_f(n,S) = 0 \tag{35}$$

is an entropy-dependent function.

The approach of c_s to c depends on the choice of $\beta_f(n,S)$. For our illustrative calculations below, some choices of $\beta_f(n,S)$ are considered.

A. Density-independent $\beta_f(n,S)$

For such a constant β_f, the integrating factor corresponding to Eq. (33) is given by

$$f(n) = \exp\left(-\beta_f \int \frac{dn}{n}\right) = n^{-\beta_f}, \tag{36}$$

and has the property

$$\frac{d}{dn}[n^{-\beta_f}\xi] = n^{-\beta_f}\frac{\beta_f m}{n}. \tag{37}$$

Integration of Eq. (37) leads to

$$\xi = \left.\frac{\partial \varepsilon}{\partial n}\right|_{S,N} = -m + c_1 n^{\beta_f}, \tag{38}$$

where c_1 is a constant of integration. A second integration results in

$$\varepsilon = -mn + \frac{c_1 n^{\beta_f+1}}{\beta_f + 1} + c_2, \tag{39}$$

with another constant of integration c_2, and therefore

$$P = c_1 \frac{\beta_f}{\beta_f + 1} n^{\beta_f+1} - c_2. \tag{40}$$

The constants c_1 and c_2 are determined by the boundary conditions

$$\varepsilon[n_f(S),S] = \varepsilon_f(S), \tag{41}$$

$$P[n_f(S),S] = P_f(S), \tag{42}$$

where n_f is the causality-fixing density, defined by Eq. (35). The functional forms of $\varepsilon(n,S)$ and $P(n,S)$ are those obtained from the original Hamiltonian density.

From Eqs. (41) and (42), we get

$$c_1 = \frac{\varepsilon_f + mn_f + P_f}{n_a^{\beta_f+1}}, \tag{43}$$

$$c_2 = \frac{1}{\beta_f + 1}[\beta_f(\varepsilon_f + mn_f) - P_f]. \tag{44}$$

Thus the energy density and the pressure are given by

$$\varepsilon = -mn + \frac{(\varepsilon_f + mn_f + P_f)}{\beta_f + 1}\left(\frac{n}{n_f}\right)^{\beta_f+1} + \frac{\beta_f(\varepsilon_f + mn_f) - P_f}{\beta_f + 1}, \tag{45}$$

$$P = \frac{\beta_f}{\beta_f + 1}(\varepsilon_f + mn_f + P_f)\left(\frac{n}{n_f}\right)^{\beta_f+1} - \frac{\beta_f(\varepsilon_f + mn_f) - P_f}{\beta_f + 1}. \tag{46}$$

The chemical potential μ is straightforwardly obtained from $\mu = \xi - TS$. Equations (45) and (46) can be used for $n \geqslant n_f$ with a fixed $\beta_f \leqslant 1$ so that causality is never violated and such that the thermodynamic identity is obeyed thus ensuring thermodynamic consistency. At this stage, we must reiterate the point that ε and P as given in Eqs. (45) and (46) are functions of (n,S). The switch to (n,T) is easily achieved by setting

$$\varepsilon(n,T) = \varepsilon[n,S(n,T)], \tag{47}$$

$$P(n,T) = P[n,S(n,T)], \tag{48}$$

$$\beta(n,T) = \beta[n,S(n,T)]. \tag{49}$$

Note that the procedure outlined above for $T \neq 0$ closely mirrors that for $T = 0$ described in Appendix E of our earlier work in Ref. [18], but with the use of appropriate quantities at finite T. The method outlined in Ref. [18] for $T \neq 0$ was flawed in that Eq. (E18) there defining the chemical potential lacked a term involving TS, that is, μ was taken to be $\partial\varepsilon/\partial n|_{S,N}$ instead of the correct $\partial\varepsilon/\partial n|_{S,V}$ where $n = N/V$. Equation (34) in this work corrects that error. Moreover, the assumption that $C_P/C_V =$ constant was made, which is only true in the degenerate limit ($S \leqslant 1$) where $C_P/C_V \simeq 1$.

B. Density-dependent $\beta_f(n,S)$

We emphasize that β_f need not be a constant. Consider, for the purposes of illustration, the function

$$\beta_f(n,S) = a_1 + \frac{a_2 n^{a_3}}{1 + a_4 n^{a_3}}, \tag{50}$$

where the a_i are real numbers; a_1 and a_3 are unitless while a_2 and a_4 have units fm^{3a_3}. For this β_f to approach 1 from below they must all be positive and $a_1 + a_2/a_4 = 1$; $a_1 > 0$ also ensures that Eq. (35) always has a solution. Moreover, if the fraction $a_2/(a_3 a_4)$ is an integer, then ξ, ε, and P are relatively simple functions of the density.

For example, if we choose $a_1 = 1/2$, $a_2 = 2$, $a_3 = 1$, and $a_4 = 4$ then

$$\beta_f = \frac{1}{2} + \frac{2n}{1+4n}, \tag{51}$$

$$\xi = -m + c_1 n^{1/2}(1+4n)^{1/2}, \tag{52}$$

$$\varepsilon = -mn + \frac{c_1}{16}\left[n^{1/2}(1+4n)^{1/2}(1+8n) - \frac{1}{2}\sinh^{-1}(2n^{1/2})\right] + c_2, \tag{53}$$

$$P = -\frac{c_1}{16}\left[n^{1/2}(1+4n)^{1/2}(1-8n) - \frac{1}{2}\sinh^{-1}(2n^{1/2})\right] - c_2. \tag{54}$$

For the choice $a_1 = 4/5$, $a_2 = 2$, $a_3 = 1/5$, and $a_4 = 10$, we get

$$\beta_f = \frac{4}{5} + \frac{2n^{1/5}}{1+10n^{1/5}}, \tag{55}$$

$$\xi = -m + c_1(n^{4/5} + 10n), \tag{56}$$

$$\varepsilon = -mn + \frac{5}{9}c_1(n^{9/5} + 9n^2) + c_2, \tag{57}$$

$$P = c_1\left(\frac{4}{9}n^{9/5} + 5n^2\right) - c_2. \tag{58}$$

Of course, many other possibilities exist for the a_i above, as well as for the generic functional form of β_f.

IV. NUMERICAL NOTES

Here we describe the procedure to calculate $(c_s/c)^2$ for the Hamiltonian density in Eq. (5) for conditions of arbitrary degeneracy. The analytical results obtained in Sec. II for the degenerate and nondegenerate cases serve as a check for the results obtained in this section. To calculate the finite-entropy properties corresponding to Eq. (5), we employ the Johns, Ellis, and Lattimer (JEL) [55] scheme in which the Fermi–Dirac integrals

$$F_\alpha = \int_0^\infty \frac{x^\alpha}{e^{x-\psi}+1}dx \tag{59}$$

are expressed as algebraic functions of a single parameter f related to the entropy via

$$S = \frac{5}{3}\frac{F_{3/2}(f)}{F_{1/2}(f)} - \psi(f), \tag{60}$$

where [18]

$$F_{3/2}(f) = \frac{3f(1+f)^{1/4-M}}{2\sqrt{2}}\sum_{m=0}^{M} p_m f^m \tag{61}$$

$$F_{1/2}(f) = \frac{f(1+f)^{1/4-M}}{\sqrt{2(1+f/a)}}\sum_{m=0}^{M} p_m f^m \times\left[1 + m - \left(M - \frac{1}{4}\right)\frac{f}{1+f}\right], \tag{62}$$

$$\psi(f) = \frac{\mu(n,S) - V(n)}{T(n,S)} = 2(1+f/a)^{1/2} + \ln\left[\frac{(1+f/a)^{1/2}-1}{(1+f/a)^{1/2}+1}\right]. \tag{63}$$

The values of the coefficients appearing in Eqs. (61)–(63) are $a = 0.433$, $M = 3$, $p_0 = 5.34689$, $p_1 = 16.8441$, $p_2 = 17.4708$, and $p_3 = 6.07364$. We note that the F_α are connected via their derivatives with respect to ψ according to $\partial F_\alpha/\partial\psi = \alpha F_{(\alpha-1)}$. The JEL scheme enables a rapid and an accurate evaluation of the thermodynamic quantities preserving thermodynamic consistency.

The kinetic-energy density τ and the number density n are related to $F_{3/2}$ and $F_{1/2}$, respectively:

$$\tau(n,S) = \frac{\gamma}{2\pi^2}\left[\frac{2m^*(n)T(n,S)}{\hbar^2}\right]^{5/2} F_{3/2}[f(S)], \tag{64}$$

$$n = \frac{\gamma}{2\pi^2}\left[\frac{2m^*(n)T(n,S)}{\hbar^2}\right]^{3/2} F_{1/2}[f(S)], \tag{65}$$

where $\gamma = 1$ (2) for PNM (SNM) and $f(S)$ is the solution of Eq. (60). From Eq. (65), it follows that

$$T(n,S) = \left(\frac{\pi^2\hbar^3}{\gamma\sqrt{2}}\right)^{2/3}\frac{n^{2/3}}{m^*(n)}\frac{1}{F_{1/2}^{2/3}[f(S)]} \tag{66}$$

and

$$\left.\frac{\partial T(n,S)}{\partial n}\right|_S = \frac{2Q(n)}{3n}T(n,S), \tag{67}$$

with $Q(n)$ given by Eq. (7). The total energy density is given by

$$\epsilon(n,S) = \mathcal{H}(n,S) + mn, \tag{68}$$

and thus

$$\left.\frac{\partial\epsilon}{\partial n}\right|_S = \frac{5}{3n}\frac{\hbar^2}{2}\frac{\tau(n,S)}{m^*(n)}\left[1 - \frac{3n}{5m^*}\frac{dm^*}{dn}\right] + \frac{dV}{dn} + m. \tag{69}$$

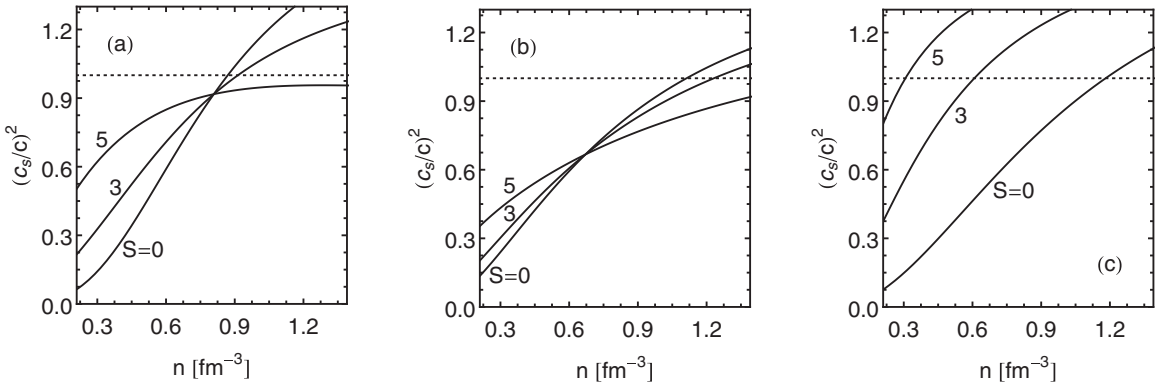

FIG. 1. Squared speed of sound vs density in PNM for the models of (a) APR, (b) LS, and (c) SLy4 at fixed entropy.

The pressure is obtained from

$$P(n,S) = n\left.\frac{\partial\epsilon}{\partial n}\right|_S - \epsilon(n,S) \tag{70}$$

$$= \frac{2}{3}\frac{\hbar^2}{2}\frac{Q(n)}{m^*(n)}\tau(n,S) + n\frac{dV}{dn} - V(n), \tag{71}$$

and therefore

$$\left.\frac{\partial P}{\partial n}\right|_S = n\frac{d^2V}{dn^2} + \frac{10}{9n}\frac{\hbar^2}{2}\frac{Q(n)}{m^*(n)}\tau(n,S) \times\left[1 - \frac{3n}{5m^*(n)}\frac{dm^*}{dn} + \frac{3n}{5Q(n)}\frac{dQ}{dn}\right]. \tag{72}$$

In the causality-fixing regime [$n \geqslant n_f(S)$], Eqs. (45) and (46) imply

$$\left.\frac{\partial\epsilon}{\partial n}\right|_S = \left.\frac{\partial\varepsilon}{\partial n}\right|_S + m = \frac{(\varepsilon_f + mn_f + P_f)}{n_f}\left(\frac{n}{n_f}\right)^{\beta_f}, \tag{73}$$

$$\left.\frac{\partial P}{\partial n}\right|_S = \frac{\beta_f}{n_f}(\varepsilon_f + mn_f + P_f)\left(\frac{n}{n_f}\right)^{\beta_f}. \tag{74}$$

Correspondingly, $(c_s/c)^2 = \beta_f$ as indicated earlier.

For the conversion of ϵ, P, and c_s to the (n,T) variables, we must first express the entropy in terms of n and T. This is accomplished by solving

$$n = \frac{\gamma}{2\pi^2}\left[\frac{2m^*(n)T}{\hbar^2}\right]^{3/2} F_{1/2}(f) \tag{75}$$

for $f(n,T)$, which is then used as input in the functions that appear in Eq. (60).

V. RESULTS

In this section, we present results pertaining to the speed of sound for the PNM models of APR [18,47], LS [45], and SLy4 [46] and the alterations caused by our causality-enforcing scheme to the properties of the neutron stars in their maximum-mass configuration. This configuration reaches the largest central density and therefore it is the setting where the effects of causality implementation will be most apparent. Our results also illustrate how various thermodynamic functions are modified by this approach in the case of PNM for the EOS of APR.

Figure 1 shows the squared speed of sound of the three models for PNM for different values of the entropy. Results for APR and LS are qualitatively similar in that for densities lower than a certain density n_X, the higher-entropy curves lie higher whereas the situation is reversed for densities $n > n_X$. Consequently, causality for finite entropies (temperatures) is violated at densities that are higher than those at zero temperature for these two models. The intersection point at intermediate densities is common to all curves (for each model) and thus independent of the entropy. Its value is obtained by solving

$$\left(\frac{c_s}{c}\right)^2_{S=0} - \left(\frac{c_s}{c}\right)^2_{S\gg1} = 0, \tag{76}$$

where the first term refers to the squared speed of sound in cold matter and the second term is given by Eq. (21).

The speed of sound of SLy4, on the other hand, is a monotonically increasing function of the entropy and hence the causality-violating density n_a decreases with increasing entropy. The n_a for the three models at $S = 0$, 3, and 5 as well as the fixed points n_X of APR and LS are given in Table I.

The differences in the results of c_s^2 for the three models are related to the behavior of the effective masses and their derivatives with respect to density as reflected in the function $Q(n)$ and its derivative with respect to density. Figure 2 shows results of m^*/m and $Q(n)$ vs density. For the LS model here, $Q(n) = 1$ because $m^*(n) = m$, the vacuum nucleon mass. For the APR and SLy4 models, m^*/m decreases monotonically with density, the variation in the latter case being substantially more than for the former. These variations are in turn reflected

TABLE I. Densities at which causality is violated at $S = 0$, 3, and 5 for APR, LS, and SLy4 in their PNM (SNM) configuration and intersection density (where applicable).

Property	APR	LS	SLy4
$n_{a,0}$ (fm^{-3})	0.870 (0.841)	1.112 (1.092)	1.181 (1.298)
$n_{a,3}$ (fm^{-3})	0.914 (0.849)	1.232 (1.165)	0.608 (0.814)
$n_{a,5}$ (fm^{-3})	2.710 (0.994)	1.774 (1.478)	0.307 (0.454)
n_X (fm^{-3})	0.809 (0.830)	0.671 (0.708)	N/A

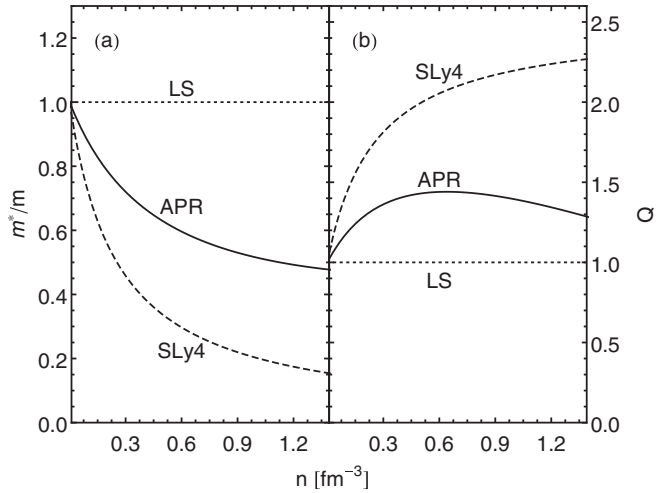

FIG. 2. The effective mass ratio m^*/m and the quantity $Q = 1 - (3n/2m^*)dm^*/dn$ vs density in PNM for the APR, LS, and SLy4 models.

in the behavior of $Q(n)$ with n for these two models. These results clearly indicate the crucial role of the density dependence of the effective mass on the speed of sound in hot, dense matter.

The physical reason why the $(c_s/c)^2$ curves for different entropies intersect at an apparently unique density n_X for the APR and LS models, but not for the SLy4 model may be understood as follows: As shown in Eq. (21), the speed of sound of nonrelativistic models with only contact interactions is independent of S or T not only for cold matter $(S, T/T_F \ll 1)$, but also in the extreme nondegenerate case $(S, T/T_F \gg 1)$. The curves of $(c_s/c)^2$ corresponding to these two limits establish the boundaries for the values that $(c_s/c)^2$ can attain as a function of (n,S) and (n,T). Thus, if this area is reduced to a point (i.e., when $c_s(n,0)$ and $c_s(n,S \gg 1)$ intersect) then all other curves must also pass through this point (no curve of intermediate T or S is allowed to exist above or below the two limits).

Models with finite-range interactions appear to have a fixed point as well (see our discussion later) but this is not necessarily the case; it is just that the range of intersection densities is rather narrow, especially in the (n,S) variables. Nevertheless, such an intersection point does not have to exist; that is, Eq. (76) does not necessarily admit a solution. Whether or not this is the case is a question of how the model-specific parametrization affects the density dependence of m^*/m and Q. If these quantities decrease relatively slowly as a function of density, as in the APR and LS models, then a fixed point is likely to exist. Such is not the case for the SLy4 model in which a rapid variation of m^*/m and Q occurs.

Tables II–IV list the maximum mass and the corresponding radius and central number density n_c, total energy density ϵ_c, and pressure P_c for different values of β_f at $T = 0$. The last column in each table displays these quantities as obtained by using the original causality-violating EOS. As β_f is increased toward 1, $M_{\max}$, n_c, ϵ_c, and P_c approach

TABLE II. PNM neutron star properties for the APR model for different values of β_f at $T = 0$.

Prop. \ β_f	0.5	0.7	0.9	Not fixed
n_f (fm^{-3})	0.547	0.667	0.796	N/A
$M_{\max}$ ($M_\odot$)	2.00	2.13	2.18	2.20
$R_{\max}$ (km)	10.61	10.46	10.31	10.16
n_c (fm^{-3})	1.107	1.096	1.101	1.111
ϵ_c (MeV fm^{-3})	1398.6	1433.3	1472.0	1507.0
P_c (MeV fm^{-3})	516.0	691.9	851.1	1005.1

their pre-implementation values from below whereas $R_{\max}$ does so from above. Changes to these quantities (compared to pre-implementation) are small; about 10% even for $\beta_f = 0.5$, with the notable exception of the central pressure P_c which nearly halves. For LS, the $\beta_f = 0.9$ star is identical to the original because $n_f(\beta_f = 0.9)$ exceeds the central density of the star. A similar consideration applies for SLy4 for which $n_f(\beta_f = 0.9)$ is relatively close to n_c.

Figure 3 shows how the squared speed of sound of APR (PNM) is altered by our method as a function of the density for fixed entropy (left panel) and for fixed temperature (right panel) for a fixed $\beta_f = 0.9$. That the different curves appear to be causally fixed at the same density is a consequence of the (accidental) fact that, for APR, $n_f(\beta_f = 0.9) \simeq n_X$. As a caution we point out that the problematic implementation of Ref. [18] will *appear* correct if one chooses $\beta_f = \beta_f(n_X)$.

A notable feature of the results in Fig. 3 is that $(c_s/c)^2 = 0.9$ for all $n \geqslant n_a$, the density at which acausality sets in for the APR model. With a density-dependent β_f, a gradual approach of $(c_s/c)^2$ to 1 may be achieved. Figure 4 shows results with the density-dependent β_f given by Eq. (51). As noted earlier, many other possibilities also exist as long as one can find a tractable, preferably analytical, solution to Eq. (33).

The implementation of causality introduces modifications to the total energy density ϵ, pressure P, chemical potential μ, specific heats C_V and C_P, and adiabatic index Γ_S, which are exhibited in Figs. 5–10, respectively. All of these results correspond to $\beta_f = 0.9$. These modifications occur at high densities and are more pronounced for quantities (P, μ, Γ_S, and C_P) that involve density derivatives of the

TABLE III. Same as Table II, but for the LS model.

Prop. \ β_f	0.5	0.7	0.9	Not fixed
n_f (fm^{-3})	0.515	0.705	0.951	N/A
$M_{\max}$ ($M_\odot$)	2.23	2.29	2.30	2.30
$R_{\max}$ (km)	12.03	11.70	11.58	11.58
n_c (fm^{-3})	0.875	0.906	0.915	0.915
ϵ_c (MeV fm^{-3})	1101.6	1175.9	1197.7	1197.7
P_c (MeV fm^{-3})	398.0	534.0	584.1	584.1

TABLE IV. Same as Table II, but for the SLy4 model.

Prop. \ β_f	0.5	0.7	0.9	Not fixed
n_f (fm^{-3})	0.634	0.825	1.048	N/A
$M_{\max}$ ($M_\odot$)	1.95	2.03	2.05	2.05
$R_{\max}$ (km)	10.46	10.20	10.03	10.00
n_c (fm^{-3})	1.150	1.173	1.195	1.196
ϵ_c (MeV fm^{-3})	1454.2	1534.4	1590.7	1594.0
P_c (MeV fm^{-3})	530.0	717.1	852.6	872.1

energy. This observation is in accordance with that made earlier regarding the central pressure of neutron stars. Results corresponding to Eq. (51) are nearly identical and are not shown here.

A. Comparison with finite-range force models

Here we contrast the above results for $(c_s/c)^2$ with those of a nonrelativistic potential model with finite-range forces at finite temperature studied in detail in Ref. [5], where results for $(c_s/c)^2$ were, however, not shown. For PNM, the energy density in this model is

$$\epsilon = 2\int \frac{d^3k}{(2\pi)^3}\frac{\hbar^2k^2}{2m} f + Au^2 + \frac{Bu^\sigma}{1+B'u^{\sigma-1}} + u\sum_{i=1,2} C_i 2\int \frac{d^3k}{(2\pi)^3}\frac{1}{\left[1+(k/\Lambda_i)^2\right]} f, \qquad (77)$$

where $u = n/n_s$, f is the usual Fermi–Dirac distribution function at finite T, and the parameters A, B, σ, C_i, B', and Λ_i are determined from constraints provided by the empirical properties of nuclear matter at n_s. Referred to as BPAL33 in Ref. [5], their numerical values are

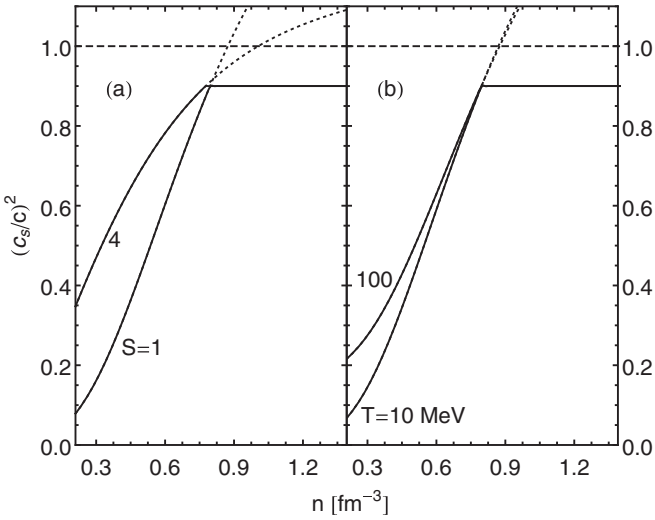

FIG. 3. Squared speed of sound in PNM for the APR model with (solid curves) and without (dotted curves) causality enforced with $\beta_F = 0.9$ for (a) fixed entropy and (b) temperature vs density.

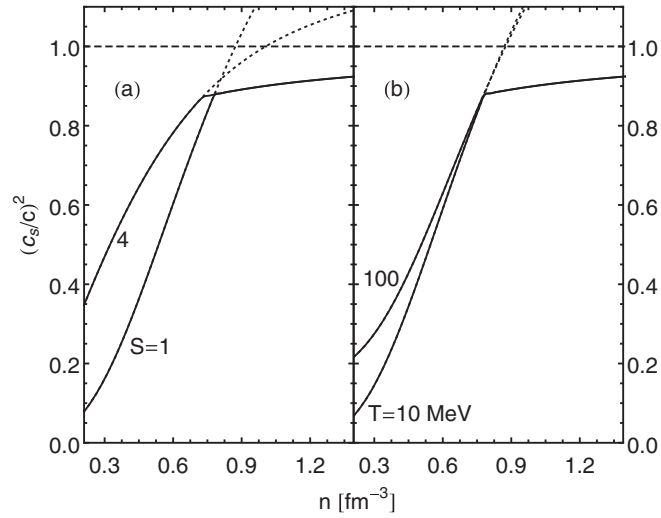

FIG. 4. Same as Fig. 3, but with the density-dependent β_f given by Eq. (51).

$A = 1.627$, $B = 8.908$, $B' = 0.422$, $C_1 = -106.7$ MeV, $C_2 = 6.544$ MeV, $\Lambda_1 = 1.5\hbar k_F^{(0)}$, and $\Lambda_2 = 3.0\hbar k_F^{(0)}$ with $k_F^{(0)} = (3\pi^2 n_s/2)^{1/3}$. Note the redefinition of parameters here from those in the original reference. The energy density in Eq. (77) differs from that of zero-range Skyrme-like models including the APR model in two respects. First, the term encapsulating the influence of higher-than-two-body forces is such that it does not lead to an acausal behavior at $T = 0$. Second, the finite-range terms lead to an effective mass

$$\frac{m^*}{m} = \left[1 + \sum_{i=1,2} \alpha_i u\left(1 + \frac{(2u)^{2/3}}{R_i^2}\right)\right]^{-1}, \qquad (78)$$

where $R_i = \Lambda_i/(\hbar k_F^{(0)})$, which saturates for $n \gg n_s$ as shown in Fig. 11. As a result, $Q < 1.2$ and $dQ/dn < 0$ for $n > n_s$ which implies that $c_s < c$ in the limit

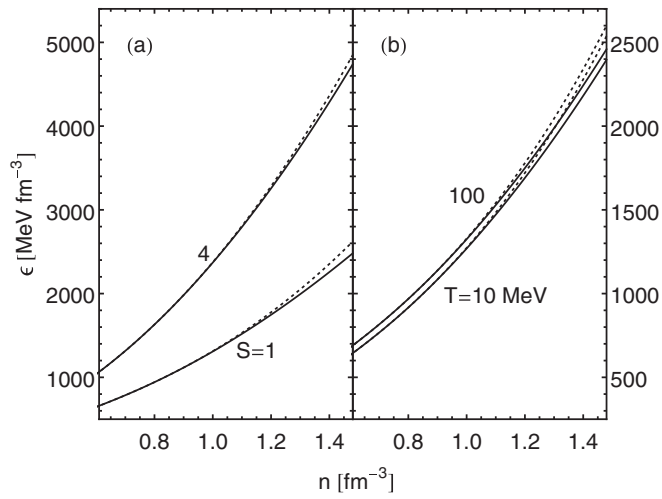

FIG. 5. Total energy density of PNM for the APR model with (solid curves) and without (dotted curves) causality enforced with $\beta_f = 0.9$ for (a) fixed entropy and (b) temperature vs density.

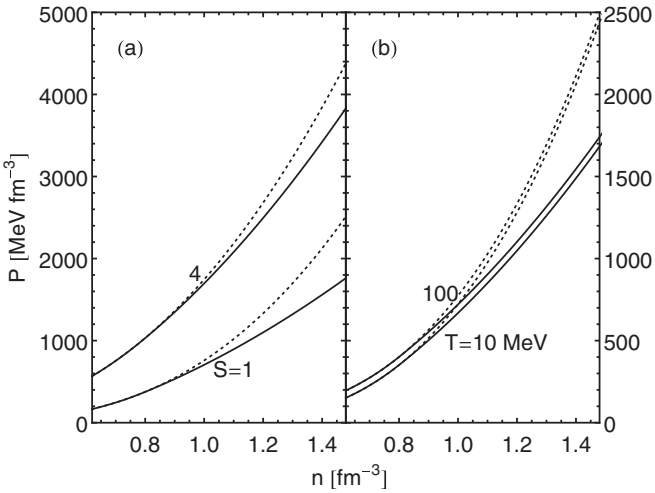

FIG. 6. Pressure of PNM for the APR model with (solid curves) and without (dotted curves) causality enforced with $\beta_f = 0.9$ for (a) fixed entropy and (b) temperature vs density.

$T \to \infty$ [Eq. (21)]. This means that $c_s < c$ for all T (see Fig. 12) being that the possible paths that c_s can traverse in (n,T) are bounded by $c_s(T = 0)$ and $c_s(T \to \infty)$. In closing this section we note that, for BPAL33, the intersection density $n_X = 0.853$ fm^{-3}.

To preserve causality, two lessons, of much value to first-principle microscopic calculations hot and dense matter, are learned from the results above. First, contributions from higher-than-two-body forces must be screened at high density at the $T = 0$ level. Second, the nucleon effective mass, which controls thermal effects, must not rapidly decrease with density as in some Skyrme-like models that employ only contact interactions. The use of finite-range forces (as in first-principle calculations of dense matter), which tends to saturate the nucleon effective mass, mitigates the influence of thermal effects in making EOSs acausal.

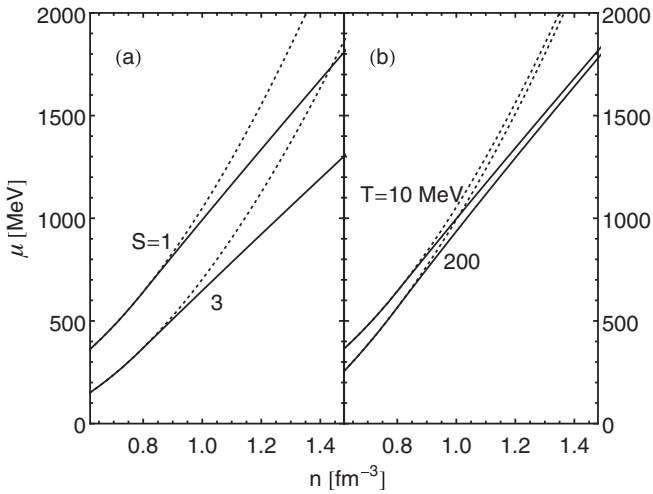

FIG. 7. Chemical potential in PNM for the APR model with (solid curves) and without (dotted curves) causality enforced with $\beta_f = 0.9$ for fixed (a) entropy and (b) temperature vs density.

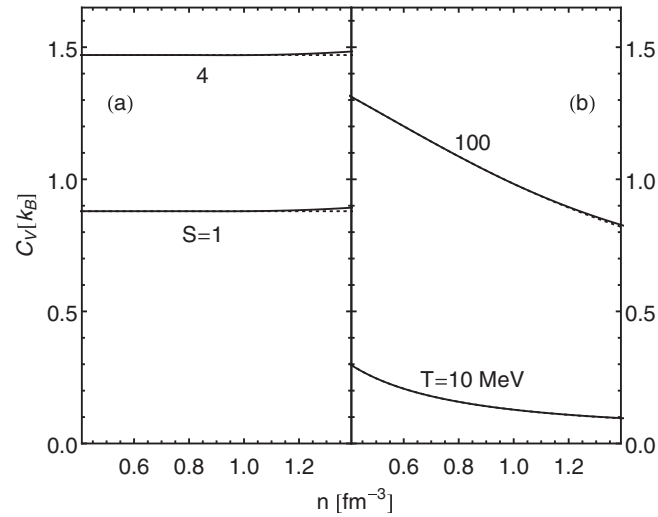

FIG. 8. Specific heat at constant volume in PNM for the APR model with (solid curves) and without (dotted curves) causality enforced with $\beta_f = 0.9$ for fixed (a) entropy and (b) temperature vs density.

VI. SUMMARY AND CONCLUSIONS

Treatments of hot, dense matter starting from a nonrelativistic Hamiltonian or Lagrangian density lead to superluminal behavior at high density as reflected in the adiabatic speed of sound exceeding that of light. This behavior will likely persist for applications in astrophysical phenomena even if the many-body problem can be solved exactly at the nonrelativistic level because Lorentz invariance is absent in such a treatment.

In this work, we propose a method by which nonrelativistic EOSs that become acausal at high densities can be modified so that they remain causal at all densities and entropies

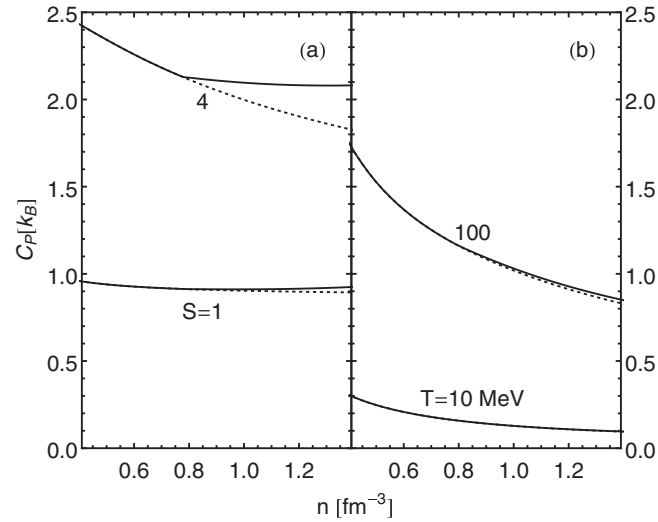

FIG. 9. Specific heat at constant pressure in PNM for the APR model with (solid curves) and without (dotted curves) causality enforced with $\beta_f = 0.9$ for fixed (a) entropy and (b) temperature vs density.

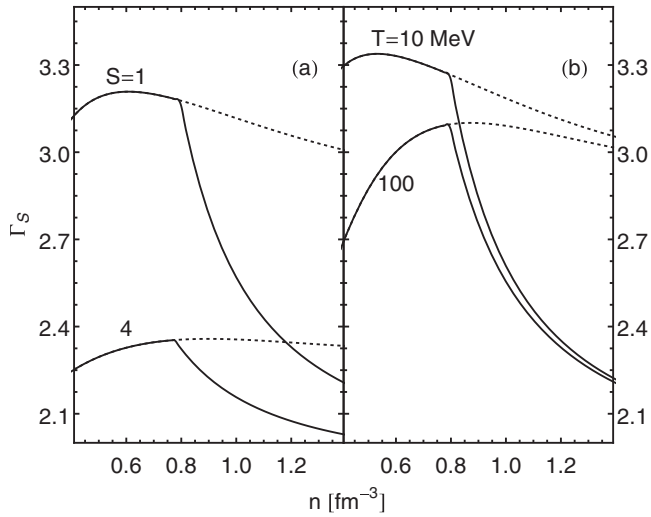

FIG. 10. Adiabatic index in PNM for the APR model with (solid curves) and without (dotted curves) causality enforced with $\beta_f = 0.9$ for fixed (a) entropy and (b) temperature vs density.

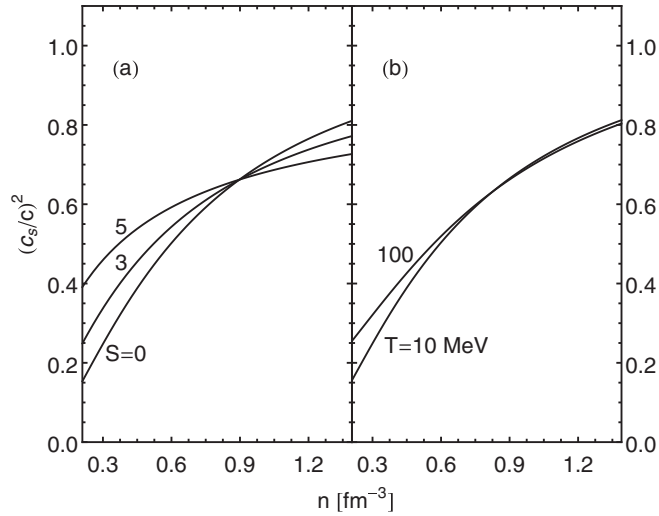

FIG. 12. Squared speed of sound in PNM for the BPAL33 model for fixed (a) entropy and (b) temperature vs density.

or temperatures. This approach is easily implemented and computationally straightforward; its most important feature is thermodynamic consistency. Illustrative calculations are presented both for a fixed value of the speed of sound c_s in the "causality-enforcement" region as well as for continuous functions of density and entropy per baryon (n,S) which approach c asymptotically from below (Figs. 3 and 4).

As examples, we explore consequences of enforcing causality to the attributes of maximum-mass neutron star configurations in pure neutron matter for the APR, LS, and SLy4 models. The EOS functions of the APR model are presented for entropies per baryon of relevance to astrophysical simulations before and after enforcing causality. Our principal findings are summarized below.

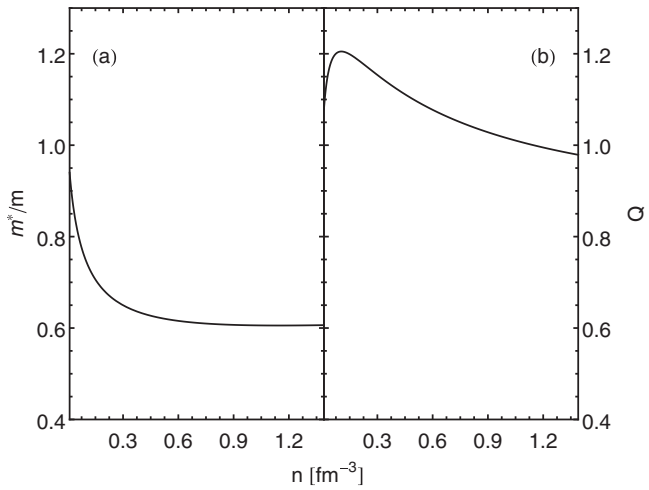

FIG. 11. The effective mass ratio m^*/m and the quantity $Q = 1 - (3n/2m^*)dm^*/dn$ vs density in PNM for the BPAL33 model.

Insofar as our choice for the "new" speed of sound c_s is close to c, we find that both cold and finite-T properties associated with the energy density ε and the specific heat at constant volume, C_V, are relatively weakly affected after enforcing causality. However, properties such as the pressure P, the chemical potential μ, and the specific heat at constant pressure, C_P, which are related to density derivatives of the energy, exhibit larger variations compared to ε and C_V. At $T = 0$, the basic characteristics of PNM-NS configurations such as their central density n_c, maximum mass $M_{\max}$, and radius of the maximum configuration $R_{\max}$, are not greatly affected by enforcing causality. However, for models (such as SLy4) in which the effective nucleon mass drops rapidly with density thermal effects cause c_s to exceed c at densities significantly lower than at $T = 0$. An interesting finding is that, in the extreme nondegenerate limit, c_s for models with contact interactions such as those considered here decouples from entropy or temperature and is instead determined by the Landau effective mass and its derivatives with respect to density.

Finally, our study of a schematic potential model illustrates that, in first-principle calculations of hot and dense matter, repulsive contributions from higher-than-two-body interactions must be screened and effective masses determined by finite-range forces must saturate at high density to preserve causality.

ACKNOWLEDGMENTS

Research support for M.P. by the U.S. DOE under Grant No. DE-FG02-93ER-40756 is gratefully acknowledged. We thank Matthias Hempel for alerting us to corrections associated with Eq. (3) in the preprint version of this paper.

[1] P. Demorest, T. Pennucci, S. Ransom, M. Roberts, and J. Hessels, Nature (London) **467**, 1081 (2010).
[2] J. Antoniadis *et al.*, Science **340**, 1233232 (2013).
[3] B. P. Abbott *et al.*, Phys. Rev. Lett. **116**, 061102 (2016).
[4] B. P. Abbott *et al.*, Phys. Rev. Lett. **116**, 241103 (2016).
[5] M. Prakash *et al.*, Phys. Rep. **280**, 1 (1997).
[6] J. M. Lattimer and A. Burrows, Astrophys. J. **307**, 178 (1986).
[7] A. Burrows, Astrophys. J. **334**, 891 (1988).
[8] H.-Th. Janka, Th. Zweger, and R. Mönchmeyer, Astron. Astrophys. **268**, 360 (1993).
[9] L. Baiotti, B. Giacomazzo, and L. Rezzolla, Phys. Rev. D **78**, 084033 (2008).
[10] L. Rezzolla, L. Baiotti, B. Giacomazzo, D. Link, and J. Font, Class. Quantum Grav. **27**, 114105 (2010).
[11] A. Bauswein, H.-T. Janka, and R. Oeschin, Phys. Rev. D **82**, 084043 (2010).
[12] M. D. Duez, F. Foucart, L. E. Kidder, C. D. Ott, and S. A. Teukolsky, Class. Quantum Grav. **27**, 114106 (2010).
[13] E. O'Connor and C. D. Ott, Astrophys. J. **730**, 70 (2011).
[14] Y. Sekiguchi, K. Kiuchi, K. Kyutoku, and M. Shibata, Phys. Rev. Lett. **107**, 051102 (2011).
[15] M. B. Deaton *et al.*, Astrophys. J. **776**, 47 (2013).
[16] K. Hotokezaka, K. Kiuchi, K. Kyutoku, T. Muranushi, Y.-I. Sekiguchi, M. Shibata, and K. Taniguchi, Phys. Rev. D **88**, 044026 (2013).
[17] F. Foucart, M. B. Deaton, M. D. Duez, E. O'Connor, C. D. Ott, R. Haas, L. E. Kidder, H. P. Pfeiffer, M. A. Scheel, and B. Szilagyi, Phys. Rev. D **90**, 024026 (2014).
[18] C. Constantinou, B. Muccioli, M. Prakash, and J. M. Lattimer, Phys. Rev. C **89**, 065802 (2014).
[19] M. Prakash, T. L. Ainsworth, and J. M. Lattimer, Phys. Rev. Lett. **61**, 2518 (1988).
[20] S. A. Bludman and C. Dover, Phys. Rev. D **22**, 1333 (1980).
[21] A. L. Fetter and J. D. Walecka, *Quantum Theory of Many-Particle Systems* (McGraw-Hill, New York, 1971).
[22] X. Zhang and M. Prakash, Phys. Rev. C **93**, 055805 (2016).
[23] B. D. Day, Rev. Mod. Phys. **50**, 495 (1978).
[24] M. Baldo, I. Bombaci, and G. F. Burgio, Astron. Astrophys. **328**, 274 (1997).
[25] F. Sammarruca, W. Barredo, and P. Krastev, Phys. Rev. C **71**, 064306 (2005).
[26] E. N. E. van Dalen, C. Fuchs, and A. Faessler, Phys. Rev. C **72**, 065803 (2005).
[27] M. Baldo, G. F. Burgio, H.-J. Schulze, and G. Taranto, Phys. Rev. C **89**, 048801 (2014).
[28] P. Armani *et al.*, J. Phys.: Conf. Ser. **336**, 012014 (2011).
[29] S. Gandolfi, J. Carlson, and S. Reddy, Phys. Rev. C **85**, 032801 (2012).
[30] G. Wlazlowski, J. W. Holt, S. Moroz, A. Bulgac, and K. J. Roche, Phys. Rev. Lett. **113**, 182503 (2014).
[31] A. Gezerlis and J. Carlson, Phys. Rev. C **81**, 025803 (2010).
[32] K. Hebeler and A. Schwenk, Phys. Rev. C **82**, 014314 (2010).
[33] L. Coraggio, J. W. Holt, N. Itaco, R. Machleidt, and F. Sammarruca, Phys. Rev. C **87**, 014322 (2013).
[34] I. Tews, T. Krüger, K. Hebeler, and A. Schwenk, Phys. Rev. Lett. **110**, 032504 (2013).
[35] H. Togashi and M. Takano, Nucl. Phys. A **902**, 53 (2013).
[36] J. E. Lynn, I. Tews, J. Carlson, S. Gandolfi, A. Gezerlis, K. E. Schmidt, and A. Schwenk, Phys. Rev. Lett. **116**, 062501 (2016).
[37] E. Epelbaum, H. Krebs, D. Lee, and U.-G. Meissner, Eur. Phys. J. A **40**, 199 (2009).
[38] J. Hu, Y. Zhang, E. Epelbaum, U.-G. Meissner, and J. Meng, arXiv:1612.05433v1.
[39] K. Hebeler, J. M. Lattimer, C. J. Pethick, and A. Schwenk, Phys. Rev. Lett. **105**, 161102 (2010).
[40] M. Baldo and L. S. Ferreira, Phys. Rev. C **59**, 682 (1999).
[41] C. Wellenhofer, J. W. Holt, N. Kaiser, and W. Weise, Phys. Rev. C **89**, 064009 (2014).
[42] A. Carbone, A. Rios, and A. Polls, Phys. Rev. C **90**, 054322 (2014).
[43] M. Nauenberg and G. Chapline, Astrophys. J. **179**, 277 (1973).
[44] J. M. Lattimer, M. Prakash, D. Masak, and A. Yahil, Astrophys. J. **355**, 241 (1990).
[45] J. M. Lattimer and F. D. Swesty, Nucl. Phys. A **535**, 331 (1991).
[46] E. Chabanat, P. Bonche, P. Haensel, J. Meyer, and R. Schaeffer, Nucl. Phys. A **635**, 231 (1998).
[47] A. Akmal, V. R. Pandharipande, and D. G. Ravenhall, Phys. Rev. C **58**, 1804 (1998).
[48] L. Landau and E. M. Lifshitz, *Fluid Mechanics*, 2nd ed. (Butterworth-Heinemann, Oxford, 1987), Vol. 6.
[49] S. Weinberg, Astrophys. J. **168**, 175 (1971).
[50] J. Guichelaar, Physica **74**, 330 (1974).
[51] M. Prakash, in *Nuclear Equation of State*, edited by A. Ansari and L. Satpathy (World Scientific, Singapore, 1996), p. 229.
[52] C. Constantinou, B. Muccioli, M. Prakash, and J. M. Lattimer, Phys. Rev. C **92**, 025801 (2015).
[53] G. Baym and C. Pethick, *Landau Fermi-Liquid Theory* (Wiley Interscience, New York, 1991).
[54] M. Prakash, T. L. Ainsworth, J. P. Blaizot, and H. Wolter, in *Windsurfing the Fermi Sea*, edited by T. T. S. Kuo and J. Speth (Elsevier, Amsterdam, 1987), Vol. II, p. 357.
[55] S. M. Johns, P. J. Ellis, and J. M. Lattimer, Astrophys. J. **473**, 1020 (1996).